Computational Materials Science 220 (2023) 112037

Contents lists available at ScienceDirect

Computational Materials Science

journal homepage: www.elsevier.com/locate/commatsci

Effects of chemical complexity on the initial oxidation resistance of $HfC_{1-x}N_x$ ceramics

Daming Yan [a], Yang Yang [a,*], Xiangdong Ding [a,*], Turab Lookman [b], Hongxiang Zong [a,*], Jun Sun [a]

[a] State Key Laboratory for Mechanical Behavior of Materials, Xi'an Jiaotong University, Xi'an 710049, China
[b] AiMaterials Research LLC, Santa Fe, NM 87501, USA

ARTICLE INFO

Keywords:
Oxidation resistance
Local chemical complexity
First-principles calculation
Machine learning
Refractory alloy ceramics

ABSTRACT

The initial oxidation process of refractory alloy ceramics is closely related to their intrinsic properties such as surface adsorption or diffusion of oxygen atoms. We devise a machine learning model that predicts the full spectrum of adsorption energies for an oxygen atom on $HfC_{1-x}N_x$ ceramic surfaces with quantum accuracy. With this approach, we show that the chemical complexity of carbonitride makes $HfC_{1-x}N_x$ ceramics exhibit multiple types of adsorption sites with competing oxygen adsorption energies, leading to fewer preferable adsorption sites. In particular, we find that heavily doped N can change the stable adsorption site from the 3-fold hollow between metals and C atoms (MMC) to the top of Hf atoms (top-Hf), and the total number of preferable adsorption sites is regulated by their competing energies. In this scenario, we predict $HfC_{0.76}N_{0.24}$ has superior anti-oxidation performance, consistent with existing experimental measurements. Our findings can stimulate new strategies to enhance the oxidation resistance of refractory alloy ceramics.

Refractory alloy ceramics (such as carbides and nitrides) have recently attracted significant interest as promising candidates for applications in extreme environments that require both high oxidation resistance and the ability to withstand significant thermal and mechanical stresses [1–4]. They are also used as thermal barrier coatings, which can effectively protect superalloy or refractory alloy matrices [5]. Of these, HfC-based ceramics are one of the most promising candidates because of their high melting points (almost 4000 °C), excellent mechanical properties and appropriate thermo-physical properties [6–8]. Nevertheless, the conventional HfC ceramics are often limited by poor oxidation resistance. For example, HfC starts to oxidize at 380–400 °C, and the oxidation weight gain is up 160 % at 600–700 °C [9]. At the same time, the solid oxides of HfO_2 are not effective oxygen barriers [10,11]. Therefore, enhancing oxidation tolerance is essential to enable high temperature structural applications for HfC-based ceramics.

In general, oxidation resistance can be enhanced by densifying oxide films upon doping. For example, the addition of Si in the HfC produced liquid Si or SiO_2 at high temperature, which can fill the holes in oxide films [12] and improve its protection to the matrix. However, the melting points of Si or SiO_2 are high, this method thus cannot take effects to prevent the oxidation behavior of HfC at low temperatures [9]. In addition, oxidation resistance can also be improved by preventing the diffusion of oxygen through structural defects such as cracks, holes and grain boundaries etc [13–16]. For instance, the oxidation resistance of dense single-crystalline HfC prepared by CVD is much better than the porous one prepared by powder metallurgy [17], although they have the same composition.

Recently, it was found that the partial substitution of N atoms at the C sites can largely improve the oxidation tolerance, even at very high temperatures. For example, Zhang et.al. [18] synthesized a series of HfC_xN_y solid solutions and evaluated their ablation resistance at 3273 K. They suggested that $HfC_{0.76}N_{0.24}$ exhibits only 10 % ablation loss compared to conventional HfC ceramics. Other solid solutions of (Ta, Hf)CN ceramics also show excellent oxidation resistance in the air [19]. Structure defects such as holes in HfCN and (Ta, Hf)CN ceramics are not reduced [18]. The addition of N does not significantly densify the oxide film upon oxidation, because N, which is the same as C, will eventually form gas (NO/NO_2). In other words, the addition of N may change its intrinsic property to improve its oxidation resistance at the initial stage. However, the underlying mechanism responsible for the improved oxidation resistance is still not fully elucidated.

In the present study, we investigate the effect of chemical complexity

* Corresponding authors.
E-mail addresses: yangymse@xjtu.edu.cn (Y. Yang), dingxd@mail.xjtu.edu.cn (X. Ding), zonghust@xjtu.edu.cn (H. Zong).

https://doi.org/10.1016/j.commatsci.2023.112037
Received 27 November 2022; Received in revised form 18 January 2023; Accepted 21 January 2023
Available online 31 January 2023

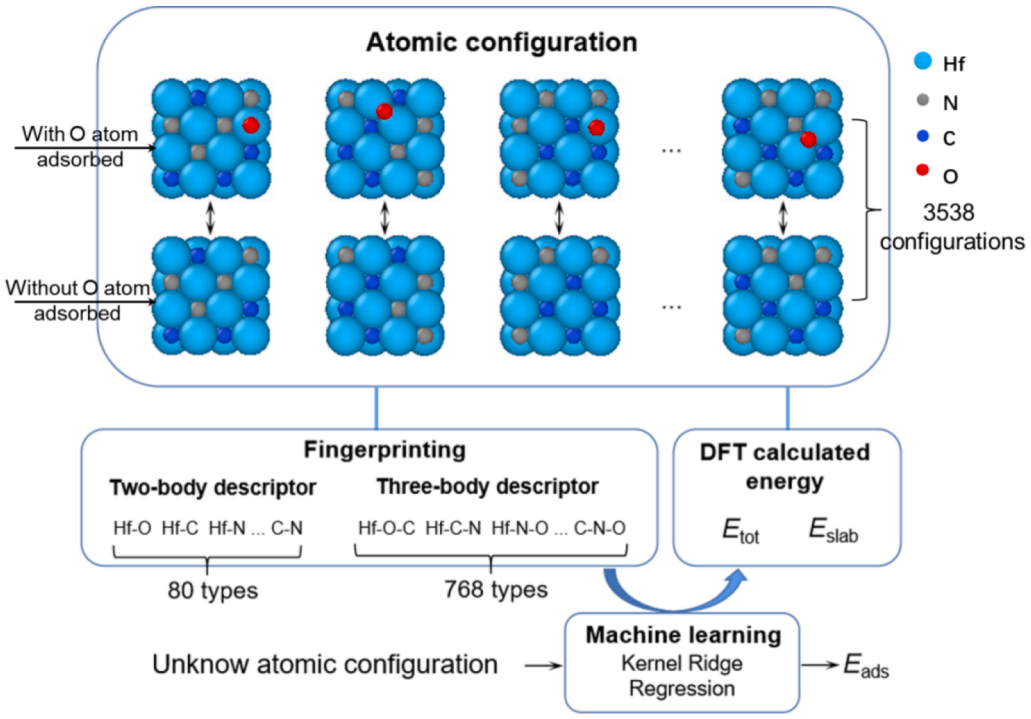

Fig. 1. Flow-chart presentation of the machine learning procedure for predicting O-adsorption energies.

by comparing the initial oxidation behavior, which is closely related to the surface adsorption and diffusion behavior, between binary HfC/HfN and ternary $HfC_{1-x}N_x$ ceramics. We find that the chemical complexity in $HfC_{1-x}N_x$ significantly reduces the total number of preferable adsorption sites and complicates diffusion pathway of oxygen atoms, thus leading to good anti-oxidation performance. Our work not only provides an atomistic understanding on the initial oxidation process for single-phase concentrated solid-solution refractory alloy ceramics, but also shows promising of designing new refractory alloy ceramics with good oxidation resistance.

Here, the initial oxidation resistance is evaluated by DFT calculations of oxygen adsorption and diffusion on ceramic surfaces. HfC, HfN, and $HfC_{1-x}N_x$ slabs with (001) surface were considered because it is very stable [20,21] and exhibits a face-centered cubic face. The slabs were created by a 5-layer 2×2 supercell with 15 Å vacuum. The bottom three layers are fixed, while the two outermost are completely allowed to relax in the DFT calculations. Atomic oxygen can bind on different high symmetry adsorption sites of the (100) surface. For each case, the position of the adsorbed oxygen atoms and the geometry of the atoms in the two outermost surface layers were fully relaxed. Once the final geometries were obtained, the adsorption energy E_{ads} was calculated by $E_{ads} = E_{tot} - E_{slab} - E_O$, where E_{tot} refers to the total energy of the system, E_{slab} refers to the energy of the structure without O adsorption, and E_O refers to the half of the total energy of an O_2 molecule.

DFT-based first-principles calculations [22,23] were carried out with the Vienna Ab-initio Simulation Package (VASP) [24,25] implemented using the generalized-gradient approximation (GGA) [26] and the projector augmented plane-wave (PAW) [27] method. Convergence tests

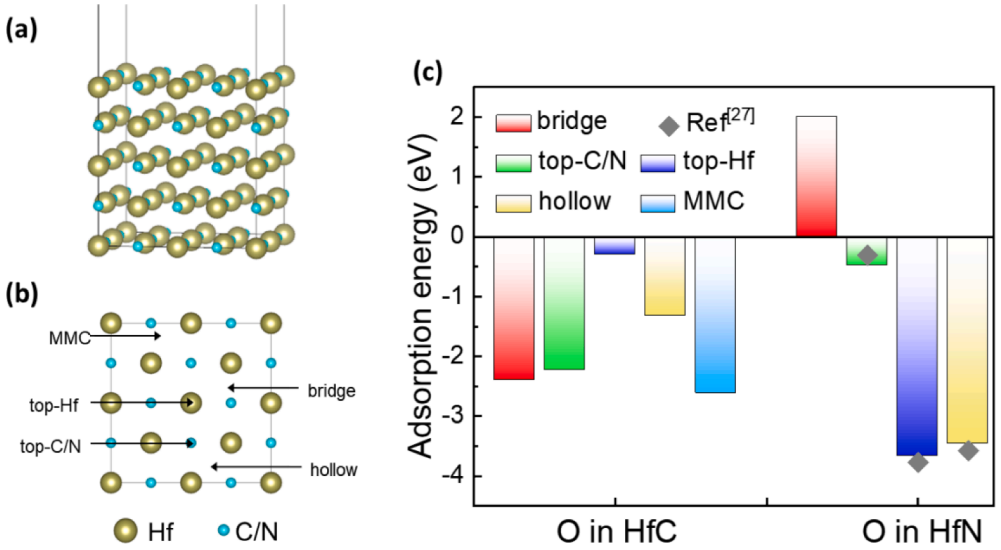

Fig. 2. (a) The slab model of HfC/HfN with a {100} free surface. (b) Adsorption sites on the {100} free surface of HfC/HfN. (c) Adsorption energy (E_{ads}) of selected adsorption sites on {100} surface of HfC and HfN.

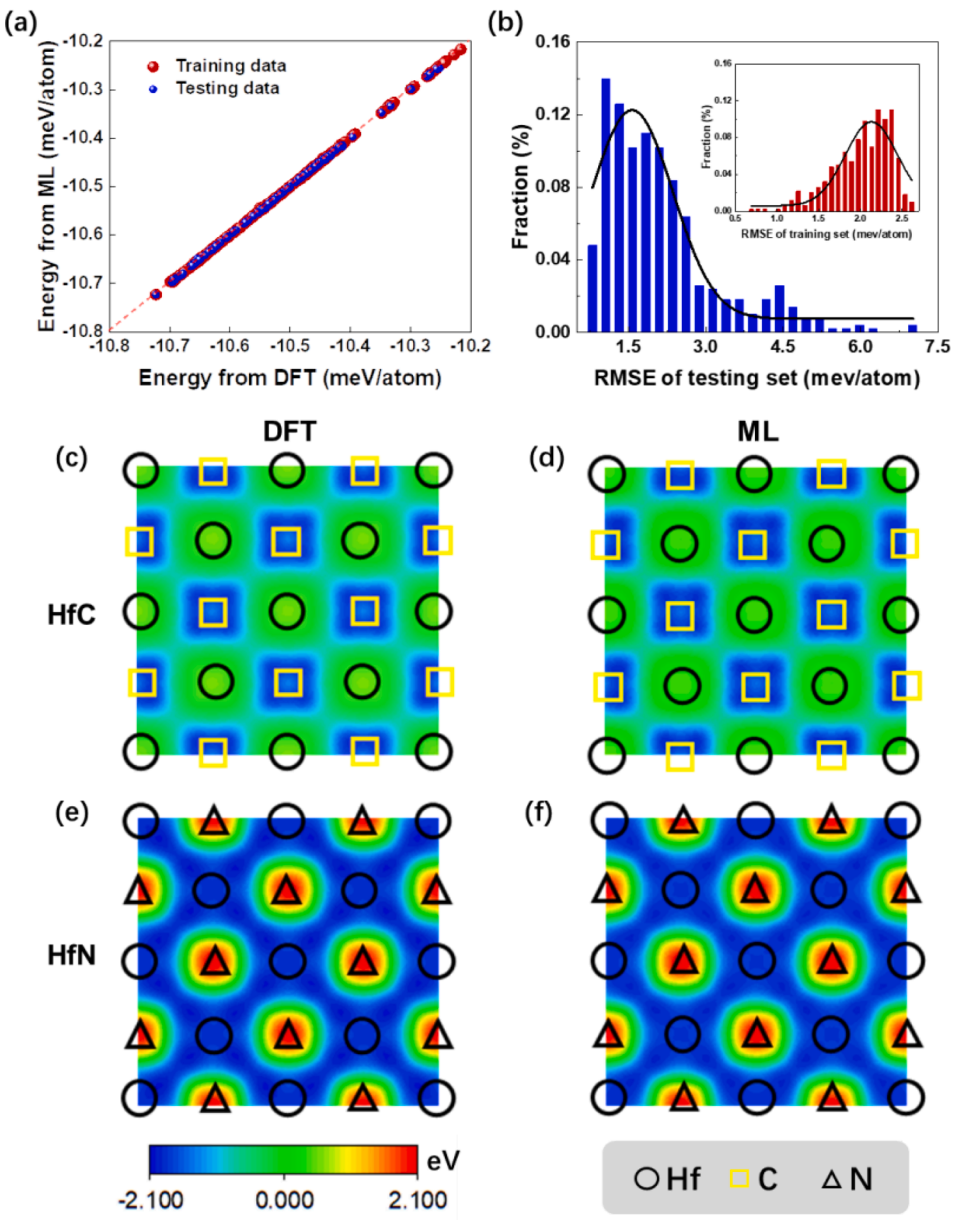

Fig. 3. (a) Comparison between the calculated and model-predicted adsorption energies. The red points and blue points show the training and testing data, respectively. (b) Blue histogram shows the RMSE distribution of the testing set in 500 models. The illustration shows the RMSE distribution of the training set. (c)-(d) DFT calculation and ML prediction of adsorption energy landscape on (001) surface of HfC ceramic. (e)-(f) DFT calculation and ML prediction of adsorption energy landscape on (001) surface of HfN ceramic. (For interpretation of the references to colour in this figure legend, the reader is referred to the web version of this article.)

for the number of K points and the plane wave cut-off energies were performed, leading to the present setting of a plane wave cutoff energy of 500 eV, and the k-point mesh [28] of $7 \times 7 \times 3$. These settings assure a total energy convergence of 0.1 meV/atom.

To overcome the computational cost of DFT calculations for $HfC_{1-x}N_x$ ceramics, we created a data-driven model for predicting the O-adsorption energies. In order to apply machine learning (ML) methods to efficiently predict energies, we performed a large number of calculations for O adsorption energies on (001) surfaces of HfC, HfN and $HfC_{1-x}N_x$ ceramics. We accumulated 3538 atomic configurations with oxygen atoms binding on different high symmetry adsorption sites, as shown in the top panel of Fig. 1. The features or descriptors for local chemical properties are extracted via a set of exponential decayed cosine functions and Gaussian smoothened radial distribution functions, and these features have proved to efficiently capture local covalent bonding [29–32]. The change of the bond length and bond angle can be described by a set of exponential decayed cosine functions (two-body descriptors) and Gaussian smoothened radial distribution functions (three-body descriptors), respectively. Combining these with the structural features yields a total number of features equal to 848 (see Fig. 1). The mapping of these features to the O-adsorption energies was achieved by applying the kernel ridge regression model. Regularization applies a penalty to large coefficients and therefore results in simpler models that are less likely to be overfitting. The optimal model with the lowest cross validation error was further used to predict the adsorption energy values. To improve reproducibility, all the DFT trajectories and corresponding machine learning model are uploaded to the GitHub site https://github.com/YOLOYDM/HfCN.

We start by studying the adsorption of atomic oxygen on the (001) surface (Fig. 2a) because of its lowest surface energy (Fig. S4), which is representative. As shown in Fig. 2b, several high-symmetry adsorption sites such as the top Hf, C and N atoms (hereafter refer to as top-Hf, top-C and top-N, respectively), the bridge site, the hollow site and the 3-fold hollow between metals and C atoms (MMC), etc. (It should be noted that oxygen atoms do not stably adsorb at the MMN position in HfN, but move to the neighboring hollow position after relaxation (Fig. S5)) have been explored at first, and the corresponding adsorption energies are shown in Fig. 2c. We find that the adsorption of oxygen atoms on the (001) surface of HfC ceramics is a largely exothermic process. The adsorption energy E_{ads} of one O atom at top-Hf, top-C, bridge, hollow

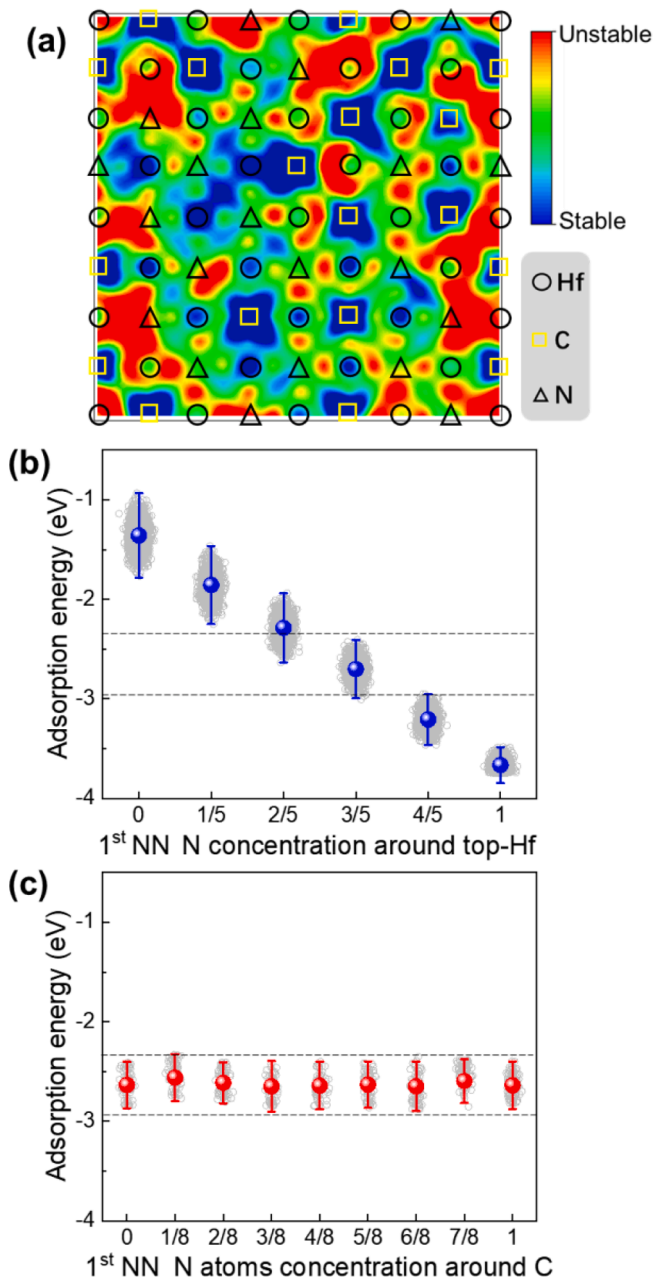

Fig. 4. (a) Energy landscape of oxygen atom adsorption on (001) plane of $HfC_{0.5}N_{0.5}$ predicted by our ML model. (b) Effect of nearest neighbor N atoms on the O-adsorption energy on MMC site. (c) Effect of nearest neighbor N atoms on the O-adsorption energy on top-Hf site.

and MMC sites are −0.36 eV, −2.28 eV, −2.46 eV, −1.39 eV and −2.62 eV, respectively. This indicates that the MMC site is the most favorable site. This is quite different from the case of HfN ceramics. On the (001) surface of HfN, the oxygen adsorption at the bridge site is an endothermic process (E_{ads} = 2.01 eV) while other oxygen adsorption sites are relatively stable or metastable with the adsorption energy E_{ads} ranging from −0.49 eV to −3.67 eV. This agrees well with previous DFT calculations [21]. More importantly, the most stable adsorption site is the top-Hf site, different from that of HfC, and the oxygen adsorption energy on HfN is much larger for the preferred sites.

We also analyzed the diffusion behavior for both HfC and HfN ceramics. The activation energies for oxygen diffusion within (001) surfaces are calculated by the nudged elastic band (NEB) method [33], as shown in Fig. S1. The corresponding energy barriers are 1.32 eV/atom (~15300 K) and 0.44 eV/atom (~5100 K), respectively. The high barrier suggests that the adsorption of atomic oxygen should dominate the initial oxidation process for HfC and HfN ceramics with work temperature lower than 3000 K. We believe it should be the same true for $HfC_{1-x}N_x$ ceramics. The random substitution of N or C atoms alters the energy landscape of O-diffusion. Previous studies have pointed out that the rough energy landscape is one of the dominant factors influencing sluggish diffusion [34].

Fig. 3 compares the O-adsorption energy from the ML prediction and DFT calculations. Fig. 3a shows the comparison of the ML model predicted E_{ads} and the DFT calculated E_{ads} for training and testing datasets, respectively. Herein, the data for training ($N_{training}$) and testing ($N_{testing}$) are randomly selected with $N_{training}$ = 2830 and $N_{testing}$ = 708. Diagonal plots of energies show good fit between ML model and DFT calculation results. To get a measure of the errors in the model, we did bootstrap sampling 500 times of the full original data. The low mean values of root mean square error (RMSE) of the training set and the testing set are 2.3 meV/atom and 1.5 meV/atom, respectively, indicating an acceptable fitting error of the present ML model (see Fig. 3b). What's more, we test the O-adsorption energy landscape on (001) surface of both HfC and HfN ceramics (see Fig. 3c-f). We also compare the results of DFT calculated oxygen adsorption energy and ML prediction on the (210) surface which has the second lowest surface energy in Fig. S6. The good agreement between ML prediction and DFT calculations proved the validity of our method on other surfaces. Further, we believe that this method can also be generalized into other systems. The excellent agreement between the DFT calculations and ML predictions further confirms the good transferability of the present ML model to various local chemical environments.

We next examined, the oxygen-adsorption behavior on $HfC_{1-x}N_x$ ceramic surfaces predicted by the ML to understand how various positions of the substitutional N atoms affect oxygen adsorption. Fig. 4a shows a typical O-adsorption energy landscape for the $HfC_{0.5}N_{0.5}$ ceramic with a 4 × 4 supercell, which includes 32 Hf atoms, 16C atoms and 16N atoms within the free surface layer. As expected, the preferable adsorption sites are strongly correlated with their local chemical environment. Although the MMC sites are still the most favorable site, the total number or density of preferable adsorption sites is sharply decreased. This is quite different from the binary HfC and HfN ceramics, both of which show O-adsorption sites with spatially uniform distribution (see Fig. 2c). More striking, some top-Hf sites become stable adsorption sites with competitive oxygen adsorption energy in the regions of high local N concentration. In other words, the concentrated solid-solution of N atoms into HfN introduces multiple types of preferable adsorption sites, and the favorable sites can be tailored by the intrinsic fluctuation of N concentration.

We further investigated the correlation between O-adsorption energy and local N concentration on $HfC_{1-x}N_x$ ceramic surfaces. We analyzed the local chemical environments around preferable adsorption sites, i.e. the MMC and top-Hf, within a given cutoff of 5.5 Å (the cutoff for the prediction of E_{ads} in our ML model). As shown in Fig. 4b, the adsorption energy on the top-Hf site, decreased linearly with the increment of its nearest neighbor (NN) N numbers. Further neighbors show rather weak influence on the E_{ads} on top-Hf (see supplementary Fig. S2). In contrast, the O-adsorption energy of MMC sites shows weak dependence on their local chemical environments, and the E_{ads} on MMC sites are in the range of −2.45 eV to −2.81 eV (Fig. 4c). Thus, the two different dependencies lead to the switching of stable O-adsorption sites with fluctuation in N concentration, i.e., the favorable O-adsorption sites change from MMC to top-Hf as the nearest neighbor N atoms exceed 3. This change can be explained by their unique electronic structures. The calculated projected density of states (PDOS) suggests that the O atom binding on top-Hf is achieved by the hybridization of O (p) and Hf (d) in the range of −1.5 to −2.5 eV, well below the Fermi level. The hybridization of O (p) and Hf (d) on the other hand moves to lower energies with increase in nearest neighbor N atoms (see supplementary Fig. S3).

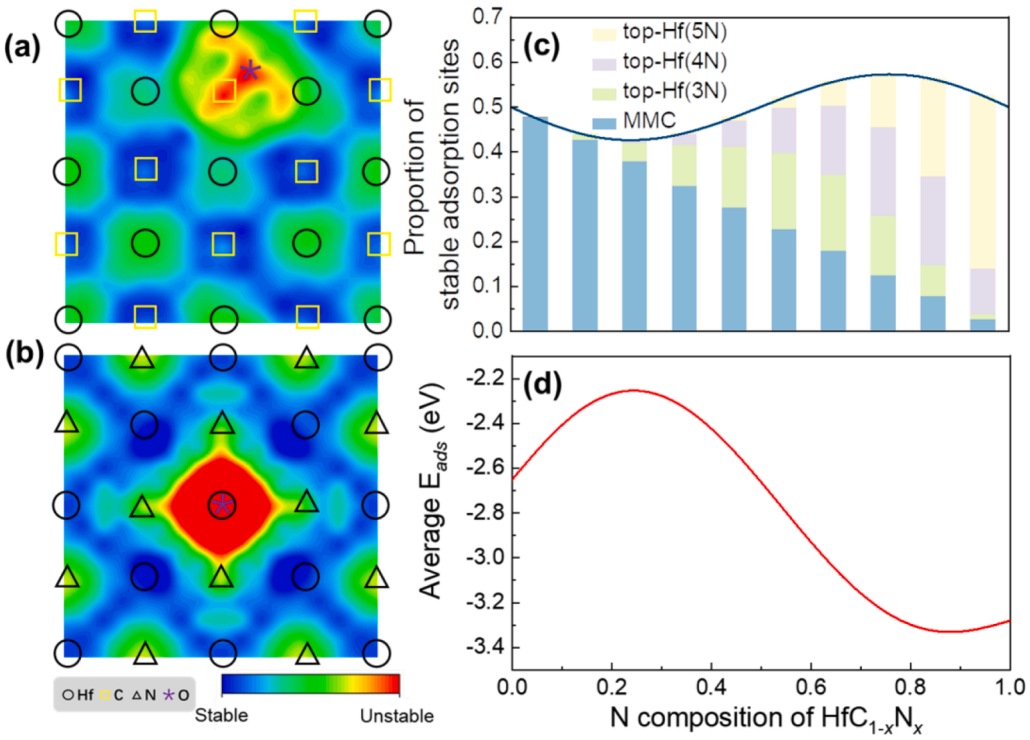

Fig. 5. (a)-(b) Energy landscape of the second oxygen atom adsorption on (0 0 1) surface of HfC or HfN ceramics. (c) The proportion of different types of stable adsorption sites with competitive oxygen adsorption energy for $HfC_{1-x}N_x$ ceramics. (d) The effective O-adsorption energy on (0 0 1) surface in $HfC_{1-x}N_x$ as a function of N concentration.

We also considered how the second oxygen atom behaves after the first O-adsorption on $HfC_{1-x}N_x$ ceramic surfaces. Fig. 5a and 5b demonstrate the energy landscape of the second-oxygen atom adsorption on (0 0 1) surfaces of HfC and HfN, respectively. For both cases, the second O-absorption can be strongly influenced only when the site is within the nearest neighbors of existing O-absorption ones, suggesting a weak effect of surface coverage for $HfC_{1-x}N_x$ ceramics. In this scenario, the oxygen-adsorption behavior on $HfC_{1-x}N_x$ ceramic surfaces can be easily estimated by counting preferable single-oxygen-atom adsorption sites. The partial substitution of N atoms at the C sites leads to a reduction of stable MMC adsorption sites. However, further increasing the stoichiometric ratio of N for $HfC_{1-x}N_x$ ceramics introduces more stable top-Hf adsorption sites. Their competition determines the total preferable adsorption sites. In other words, the adsorption of atomic oxygen for $HfC_{1-x}N_x$ ceramics is a function of their configurational entropy, i.e., the mixing entropy for an ideal solution [35].

Fig. 5c shows the statistics of stable O-adsorption sites on (0 0 1) surfaces of $HfC_{1-x}N_x$. As we increase the stoichiometric ratio of N, the number of MMC sites decreases linearly (blue bars in Fig. 5c). In contrast, the probability of top-Hf sites follows a binomial distribution of $\sum_{n\geq 3}^{5}\binom{5}{n}x^n\cdot(1-x)^{5-n}$. The possible top-Hf sites with different nearest neighbor N atoms are shown by the green, purple and yellow bars in Fig. 5c. Combining the two types of O-adsorption sites together, we can obtain the total number of preferable O-adsorption sites (the blue curve in Fig. 5c). The corresponding probability distribution function suggest the best stoichiometric ratio of $x = 0.2403$ with minimum adsorption sites on (0 0 1) surfaces of $HfC_{1-x}N_x$ ceramics. This is further confirmed by the curve of weighted average adsorption energy in Fig. 5d. It is important to point out that our prediction is consistent with recent experimental findings on the anti-oxidation measurement of $HfC_{1-x}N_x$ ceramics [18].

In summary, we have investigated the atomistic mechanism of the initial oxidation in $HfC_{1-x}N_x$ ceramics by quantum accurate machine learning model using DFT data. We show that the effect of the chemical complexity plays a critical role in the initial oxidation resistance, i.e., the random distribution of N atoms can result in the switching of preferable O-adsorption sites between MMC and top-Hf, giving rise to the reduction of stable O-adsorption sites. Such an effect leads to superior anti-oxidation performance of $HfC_{0.76}N_{0.24}$, consistent with existing experimental observations. Recently high-entropy or complex concentrated refractory alloy ceramics have emerged as a relatively new category of materials. These provide a wider space and stage to test the present findings experimentally. In addition, the combination of our findings and preexisting methods, e.g. densifying the oxide films or improving the quality of samples, may lead to better oxidation resistance.

CRediT authorship contribution statement

Daming Yan: Writing – original draft, Conceptualization, Methodology, Data curation. **Yang Yang:** Funding acquisition, Writing – review & editing, Data curation, Methodology. **Xiangdong Ding:** Funding acquisition, Writing – review & editing, Resources. **Turab Lookman:** Writing – review & editing. **Hongxiang Zong:** Funding acquisition, Writing – review & editing, Resources, Conceptualization. **Jun Sun:** Funding acquisition, Writing – review & editing, Resources.

Declaration of Competing Interest

The authors declare that they have no known competing financial interests or personal relationships that could have appeared to influence the work reported in this paper.

Data availability

Data will be made available on request.

Acknowledgments

This work was supported by Key Technologies R&D Program

(2022YFB3707601), the National Natural Science Foundation of China (Nos. 12104355, 52171011, 51320105014, 51871177, and 51931004), the China Postdoctoral Science Foundation (No. 2020M673385 and No. 2022M722508), and the 111 project 2.0 (No. BP2018008).

Appendix A. Supplementary material

Supplementary data to this article can be found online at https://doi.org/10.1016/j.commatsci.2023.112037.

References

[1] Y. Katoh, G. Vasudevamurthy, T. Nozawa, L.L. Snead, Properties of zirconium carbide for nuclear fuel applications, J. Nucl. Mater. 441 (2013) 718–742.
[2] E. Wuchina, E. Opila, M. Opeka, W.G. Fahrenholtz, I.G. Talmy, UHTCs: Ultra-High Temperature Ceramic Materials for Extreme Environment Applications, Electrochem.Soc.Interface. 16 (2007) 30–36.
[3] M.M. Opeka, I.G. Talmy, J.A. Zaykoski, Oxidation-based materials selection for 2000°C plus hypersonic aerosurfaces: Theoretical considerations and historical experience, J. Mater. Sci. 39 (2004) 5887–5904.
[4] G.V. Samsonov, I. ViniťSKiĭ, Handbook of refractory compounds, 1980.
[5] N.P. Padture, M. Gell, E.H. Jordan, Thermal barrier coatings for gas-turbine engine applications, Science 296 (2002) 280–284.
[6] G. Gruzalski, S.C. Lui, D. Zehner, Work-function changes accompanying changes in composition of (100) surfaces of HfCx and TaCx, Surf. Sci. 239 (1990) L517–L520.
[7] O. Cedillos-Barraza, D. Manara, K. Boboridis, T. Watkins, S. Grasso, D. D. Jayaseelan, R.J. Konings, M.J. Reece, W.E. Lee, Investigating the highest melting temperature materials: A laser melting study of the TaC-HfC system, Sci. Rep. 6 (2016) 1–11.
[8] Q.J. Hong, A. Van De Walle, Prediction of the material with highest known melting point from ab initio molecular dynamics calculations, Phys. Rev. B 92 (2015), 020104.
[9] S.J. Shimada, A thermoanalytical study on the oxidation of ZrC and HfC powders with formation of carbon, Solid State Ion. 149 (2002) 319–326.
[10] C.B. Bargeron, R.C. Benson, X-ray microanalysis of a hafnium carbide film oxidized at high temperature, Surf. Coat. Tech. 36 (1988) 111–115.
[11] C.B. Bargeron, R.C. Benson, R.W. Newman, A.N. Jette, T.E. Phillips, Oxidation mechanisms of hafnium carbide and hafnium diboride in the temperature range 1400 to 2100 ℃, Johns Hopkins APL Tech. Dig. 14 (1993) 1.
[12] S. Kou, S. Fan, X. Ma, Y. Ma, C. Luan, J. Ma, C. Liu, Ablation performance of C/HfC-SiC composites with in-situ HfSi2/HfC/SiC multi-phase coatings under 3000℃ oxyacetylene torch, Corros. Sci. 200 (2022), 110218.
[13] H. Ouyang, C. Li, J. Huang, L. Cao, F. Jie, L. Jing, Z. Xu, Self-healing ZrB2–SiO2 oxidation resistance coating for SiC coated carbon/carbon composites, Corros. Sci. 110 (2016) 265–272.
[14] H. Dugdale, D. Armstrong, E. Tarleton, S.G. Roberts, S. Lozano-Perez, How oxidized grain boundaries fail, Acta Mater. 61 (2013) 4707–4713.
[15] A. Stratulat, D.E.J. Armstrong, S.G. Roberts, Micro-mechanical measurement of fracture behaviour of individual grain boundaries in Ni alloy 600 exposed to a pressurized water reactor environment, Corros. Sci. 104 (2015) 9–16.
[16] K. Fujii, T. Miura, H. Nishioka, K. Fukuya. Degradation of Grain Boundary Strength by Oxidation in Alloy 600, Springer, Cham, 2011, pp. 1447–1461.
[17] C.B. Bargeron, R.C. Benson, A.N. Jette, T.E. Phillips, Oxidation of hafnium carbide in the temperature range 1400–2060°C, J. Am. Ceram. Soc. 76 (2005) 1040–1046.
[18] Z. Peng, W. Sun, X. Xiong, Y. Xu, Z. Zhou, Z. Zhan, H. Zhang, Y. Zeng, Novel nitrogen-doped hafnium carbides for advanced ablation resistance up to 3273 K, Corros. Sci. 189 (2021), 109623.
[19] V. Buinevich, A. Nepapushev, D. Moskovskikh, K. Kuskov, S. Yudin, A. Mukasyan, Ultra-high-temperature tantalum-hafnium carbonitride ceramics fabricated by combustion synthesis and spark plasma sintering, Ceram. Int. 47 (2021) 30043–30050.
[20] F. Viñes, C. Sousa, F. Illas, P. Liu, Density functional study of the adsorption of atomic oxygen on the (001) surface of early transition-metal carbides, J. Phys. Chem. C 111 (2007) 1307–1314.
[21] F. Guo, J. Wang, Y. Du, J. Wang, S.L. Shang, First-principles study of adsorption and diffusion of oxygen on surfaces of TiN, ZrN and HfN, Appl. Surf. Sci. 452 (2018) 457–462.
[22] P. Hohenberg, W. Kohn, Inhomogeneous electron gas, Phys. Rev. 136 (1964) B864.
[23] W. Kohn, L.J. Sham, Self-consistent equations including exchange and correlation effects, Phys. Rev. 140 (1965) A1133.
[24] G. Kresse, J. Furthmüller, Efficiency of ab-initio total energy calculations for metals and semiconductors using a plane-wave basis set, Comp. Mater. Sci. 6 (1996) 15–50.
[25] G. Kresse, J. Furthmüller, Efficient iterative schemes for ab initio total-energy calculations using a plane-wave basis set, Phys. Rev. B 54 (1996) 11169.
[26] J.P. Perdew, K. Burke, M. Ernzerhof, Generalized gradient approximation made simple, Phys. Rev. Lett. 77 (1996) 3865.
[27] P.E. Blöchl, Projector augmented-wave method, Phys. Rev. B 50 (1994) 17953.
[28] H.J. Monkhorst, J.D. Pack, Special points for Brillouin-zone integrations, Phys. Rev. B 13 (1976) 5188.
[29] H. Zong, G. Pilania, X. Ding, G.J. Ackland, T. Lookman, Developing an interatomic potential for martensitic phase transformations in zirconium by machine learning, NPJ Comput. Mater. 4 (2018) 1–8.
[30] Y. Yang, H. Zong, J. Sun, X. Ding, Rippling ferroic phase transition and domain switching in 2D materials, Adv. Mater. 33 (2021) 2103469.
[31] Y. Yang, L. Zhao, C.-X. Han, X.D. Ding, T. Lookman, J. Sun, H.X. Zong, Taking materials dynamics to new extremes using machine learning interatomic potentials, J. Mater. Inform. 1 (2021) 10.
[32] Y. Yang, H. Zong, X. Ding, J. Sun, Size-dependent ferroic phase transformations in GeSe nanoribbons, Appl. Phys. Lett. 121 (2022), 122903.
[33] H. Jónsson, G. Mills, K.W. Jacobsen, Nudged elastic band method for finding minimum energy paths of transitions, WORLD SCIENTIFIC (1998) 385–404.
[34] Y.J. Wang, J.P. Du, S. Shuhei, L.H. Dai, O. Shigenobu, A free energy landscape perspective on the nature of collective diffusion in amorphous solids, Acta Mater. 157 (2018) 165–173.
[35] S. Allen, T. Eagar, Thermodynamics and Kinetics of Materials, 2006.